Engineering magnetic topological insulators in $Eu_5M_2X_6$ Zintl compounds

Nicodemos Varnava,[1,*] Tanya Berry,[2,3,4] Tyrel M. McQueen,[2,3,4] and David Vanderbilt[1]
[1]*Department of Physics and Astronomy, Rutgers University, Piscataway, New Jersey 08854, USA*
[2]*Institute for Quantum Matter and William H. Miller III Department of Physics and Astronomy, The Johns Hopkins University, Baltimore, Maryland 21218, USA*
[3]*Department of Chemistry, The Johns Hopkins University, Baltimore, Maryland 21218, USA*
[4]*Department of Materials Science and Engineering, The Johns Hopkins University, Baltimore, Maryland 21218, USA*

(Received 4 April 2022; accepted 7 June 2022; published 21 June 2022)

Magnetic topological insulators provide a prominent material platform for quantum anomalous Hall physics and axion electrodynamics. However, the lack of material realizations with cleanly gapped surfaces hinders technological utilization of these exotic quantum phenomena. Here, using the Zintl concept and the properties of nonsymmorphic space groups, we computationally engineer magnetic topological insulators. Specifically, we explore $Eu_5M_2X_6$ (M=metal, X=pnictide) Zintl compounds and find that $Eu_5Ga_2Sb_6$, $Eu_5Tl_2Sb_6$, and $Eu_5In_2Bi_6$ form stable structures with nontrivial $\mathbb{Z}_2$ indices. We also show that epitaxial and uniaxial strain can be used to control the $\mathbb{Z}_2$ index and the bulk energy gap. Finally, we discuss experimental progress towards the synthesis of the proposed candidates and provide insights that can be used in the search for robust magnetic topological insulators in Zintl compounds.

DOI: 10.1103/PhysRevB.105.235128

I. INTRODUCTION

Topology and symmetry have played a profound role in shaping modern condensed matter physics and materials science. One of the most paradigmatic example is the three-dimensional (3D) $\mathbb{Z}_2$ topological insulators (TIs) protected by time-reversal symmetry [1,2]. Owing to their bulk band topology, these insulators possess an odd number of massless Dirac fermions with spin-momentum locking at their surfaces.

Although 3D topological insulators were originally proposed in time-reversal invariant systems, the $\mathbb{Z}_2$ index can also be protected by a symmetry other than simple time reversal (TR) [3,4]. These symmetries are comprised of the proper rotations composed with TR and the improper rotations not composed with TR, and are known as axion-odd symmetries [5]. If one or more axion-odd symmetry is present in the magnetic point group, then the $\mathbb{Z}_2$ index is well defined, and if this index is nontrivial we refer to it as a "magnetic TI" or equivalently an "axion insulator." In the topological phase, if a surface respects any axion-odd symmetry, then the surface has necessarily an odd number of Dirac cones. If none of the axion-odd symmetries are good symmetries of the surface, the surface can be gapped. In this case, the surface will exhibit half-integer anomalous Hall conductivity (AHC), whose sign is determined by details of the magnetic order at the terminating surface. Manipulation of the surface termination and magnetic order can give rise to unidirectional one-dimensional (1D) channels at hinges, surface steps, and surface domain walls [6–8]. Their protection from backscattering by the surface gap, the absence of external magnetic fields, and the existence of robust and controllable quantum point junctions [9] make antiferromagnetic (AFM) TIs a prominent future material platform for quantum Hall physics. Furthermore, if all surfaces are gapped and have the same sign of the surface AHC (in a global sense), then the long-sought topological magnetoelectric effect can be observed, for which an applied electric field induces a parallel magnetization and a magnetic field induces a parallel electric polarization with a quantized constant of proportionality given by $e^2/2h$.

The realization of magnetic TIs has recently become the focus of intense research [10–12] with various candidates appearing in the literature [13–21]. The most prominent, $MnBi_2Te_4$ [13,14], is a layered tetradymite compound with an A-type AFM order, i.e., with magnetization uniform in-plane but alternating from plane to plane along the stacking direction. This configuration breaks time-reversal symmetry, but importantly, it is symmetric under a time-reversed half-translation. This is an axion-odd symmetry, and since it is broken on the (001) surface, that surface can be gapped, while the side surfaces preserve the symmetry and are therefore forced to be gapless. Control over the surface termination on thin films of $MnBi_2Te_4$ has resulted in the realization of high-temperature quantum anomalous Hall effect [22] as well as axion insulating states [23]. However, with the nature and existence of surface gaps still disputed [11,16], there is an evident need for improvement in the crystal quality as well as the search for new material candidates.

To this end, a class of materials known as Zintl compounds has attracted the attention of the scientific community as promising in realizing magnetic TIs. These are defined as valence precise intermetallic phases in which electropositive cations donate electrons to covalently bonded polyanions [24]. Numerous such compounds have already been synthesized

*Corresponding author: nvarnava@physics.rutgers.edu

and characterized, featuring a variety of interesting physical properties including superconductivity [25], magnetoresistance [26], and thermoelectricity [27]. Of particular interest in the search for magnetic TIs are the Zintls, in which the role of the cation is played by a divalent Eu^{2+} and the magnetism comes from the localized, spin-polarized f-orbital manifold. Examples of Eu-based Zintls appearing in the literature as candidate magnetic TIs include $EuIn_2As_2$ [15], $EuSn_2As_2$ [16], $EuCd_2As_2$ [18], $Eu_5In_2Sb_6$ [20], and $EuSn_2P_2$ [21].

In this work, we gain insight into why Zintls are such a promising platform, and then use this understanding to engineer magnetic TIs in $Eu_5M_2X_6$ ("526") Zintls where M=Ga,In,Tl is a metal and X=As,Sb,Bi is a pnictide. The insight relies on the notion of the complete electron transfer (CET) limit. In this limit, a Zintl should be a trivial insulator, but in fact there is electron competition between cations and polyanions. In this way, Zintl compounds form complex crystal and band structures that depend strongly on the geometry of the cations and polyanions. For topologically nontrivial Zintls, the presence of a spin-orbit coupling (SOC) induced bulk gap implies that the compound is away from the CET limit. The need to move away from the CET limit to obtain nontrivial topology, motivates us to use chemical substitution and structural perturbations to modify the crystal structure geometry and control the bands close to the Fermi level.

This insight was gained in part due to the discrepancy between our calculations on $Eu_5In_2Sb_6$ and those of Rosa *et al.* [20], who suggested that it has a nontrivial $\mathbb{Z}_2$ index. Our calculations on the compound clarify that it in fact has a trivial $\mathbb{Z}_2$ index. After private communications with the authors of Ref. [20], the discrepancy was identified to stem from a single transcription error in the cif file which was obtained from Park *et al.* [28]. Having understood the geometrical implications of the discrepancy, we use $Eu_5In_2Sb_6$ as our starting point to computationally design new magnetic TIs in the 526 Eu-based family of Zintl compounds. We achieve this by means of chemical substitution and epitaxial as well as uniaxial strain to control both the bulk band inversions and bulk energy gaps. Specifically, our theory indicates that $Eu_5Ga_2Sb_6$, $Eu_5Tl_2Sb_6$, and $Eu_5In_2Bi_6$ form dynamically stable structures with nontrivial $\mathbb{Z}_2$ indices, and that epitaxial and uniaxial strain can be used to control their bulk energy gaps. However, the exact energy gaps are sensitive to the crystal structure and the magnetic configuration, which are not well established.

With this motivation, we attempted the synthesis of the $Eu_5Ga_2Sb_6$ compound, but were not successful in isolating it as a pure phase. We then set out to explore the limit of stability of Ga substituted $Eu_5(In_{2-x}Ga_x)_2Sb_6$ and find an upper solubility limit of $x \approx 0.4$ based on polycrystalline synthesis. We find that the c lattice constant contracts as the Ga concentration is increased, indicating a movement away from the CET limit in a way that is anticipated to push $Eu_5In_2Sb_6$ towards a magnetic topological insulating state.

II. COMPUTATIONAL DETAILS

Density functional theory [29,30] (DFT) based first-principles calculations were performed using the projector augmented-wave (PAW) method as implemented in the VASP code [31,32]. We used the Perdew-Burke-Ernzerhof exchange-correlation functional as parametrized by Perdew-Burke-Ernzerhof [33]. The Brillouin zone sampling was performed by using a $11 \times 3 \times 15$ k mesh for $Eu_5In_2Bi_6$ and $5 \times 5 \times 15$ for all other compounds. The energy cutoff is chosen 1.5 times as large as the values recommended for the relevant PAW pseudopotentials. SOC was included self-consistently. The Eu $4f$ states were treated by employing the GGA+U approach with the U value set to 5.0 eV.

Structure relaxation calculations were performed using the ISIF=3 tag for which forces and the stress tensor are calculated and all degrees of freedom are relaxed. To model the effect of uniaxial strain, one of the lattice constants was fixed and all other degrees of freedom were allowed to relax. Similarly we modeled epitaxial strain by fixing two of the lattice constants and allowing all other degrees of freedom to relax. Phonon calculations were carried out using the PHONOPY package [34]. Irreducible representations and their traces were calculated using Irvsp [35]. Band structure plots were obtained using PyProcar [36].

III. $Eu_5In_2Sb_6$

A. Background

The Zintl compound $Eu_5In_2Sb_6$ is a narrow-gap insulator that crystallizes in the orthorhombic space group (SG) *Pbam* (55) [28]. The prominent structural features are $[InSb_4]$ (approximate) tetrahedra that form pairs in the *ab* plane through a short Sb-Sb bond [Fig. 1(a)]. Following the Zintl concept, these tetrahedra pairs form covalently bonded polyanions $[In_2Sb_6]^{10-}$ while the divalent Eu atoms are dispersed between the polyanions providing the positive balancing charge $5[Eu^{2+}]$. Along the c axis the polyanions form quasi -1D chains via sharing tetrahedra corners (Sb_1) [Fig. 1(b)]. The compound has a layered structure along the c axis with integer layers composed of Eu and Sb_1 and half-integer layers composed of In, Sb_2, and Sb_3 [Fig. 1(b)]. This picture implies that in the CET limit, close to the Fermi level, the valence bands will have Sb-p character while those in the conduction will have Eu-d character.

With respect to magnetism, the divalent Eu atoms have fully polarized $4f$ orbitals with localized magnetic moments. The compound undergoes two magnetic transitions, at 14 and 7 K. The moments are believed be antiferromagnetically aligned in the *ab* plane, but the exact configuration still remains elusive. Importantly, the $4f$ states lie far from the Fermi level E_F, in a narrow window $[-1.7\ \text{eV}, -1.3\ \text{eV}]$. Thus treating them as core electrons has only a modest effect on the bulk bands near E_F.

The separation between the electronic and magnetic energy scales, the Zintl concept, and the layered structure with all the Eu^{2+} cations in the integer layers, point towards engineering of magnetic TIs. Namely, by setting the Eu f electrons in the core we will consider the paramagnetic phase of Eu^{2+}, and use chemical substitution and structural perturbations such as epitaxial and uniaxial strain to tune the electronic band structure away from the CET limit and into the topological phase. In addition to tuning the topological phase, we will choose conditions under which the global energy gap is optimal. Since magnetism is not included in the calculation,

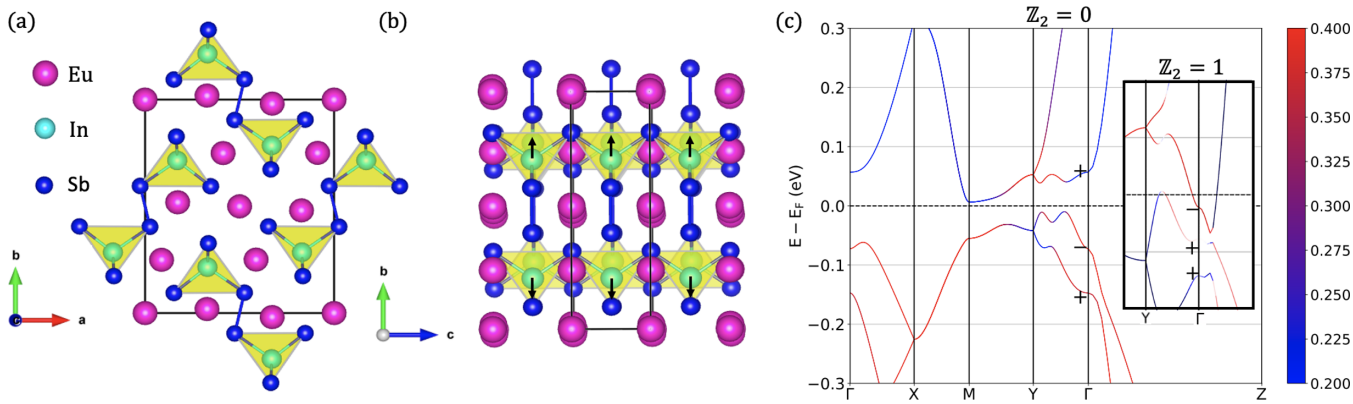

FIG. 1. Atomic and electronic structure of $Eu_5In_2Sb_6$. (a) The polyanions $[In_2Sb_6]^{-10}$ are comprised of pairs of approximate tetrahedra formed by Sb atoms and an In atom at their center. (b) Along the c axis, the corner-sharing tetrahedra form a quasi-1D chain. Eu and Sb_1 are located at integer layers while Sb_2, Sb_3, and In atoms are located at half-integer layers. Arrows indicate the direction along which the In atoms were displaced. (c) Electronic band structure of nonmagnetic (Eu f electrons in the core) $Eu_5In_2Sb_6$ in the presence of SOC. Inset shows the reproduced band structure from Rosa *et al.* [20], in which case the displacement of the In atoms causes the $\mathbb{Z}_2$ index to change.

the computational problem is greatly simplified. Recall that the topological index we are concerned with is the strong $\mathbb{Z}_2$ index of 3D TR invariant insulators which is symmetry indicated [37–40] and can be easily determined using the computational tools of topological quantum chemistry [35,41,42]. As we explain in the Supplemental Material [43] (see, also, Refs. [15,20,37,39,44–51] therein), the symmetry properties of the nonsymmorphic SG 55 allow the determination of the topology just from the knowledge of inversion eigenvalues at Γ and Z. In addition, the large energy gap at the $k_z = \pi$ plane, of the order of 1.5 eV, implies that no band inversion will occur at the Z point. This offers an extra degree of robustness since we can focus on causing a band inversion at the Γ point without worrying about band inversions at the Z point.

As we explained in the Introduction, the magnetic configuration and its symmetry properties have important implications for the surfaces. However, the complex nature of the magnetic structure of $Eu_5In_2Sb_6$, with ten Eu atoms coming in three symmetry-independent groups, makes a prediction based on first-principles calculations very difficult. In an upcoming work, we use both first-principles calculations and neutron diffraction experiments to determine the magnetic configurations of $Eu_5In_2Sb_6$.

B. The band structure

In Fig. 1(c) we show the band structure of $Eu_5In_2Sb_6$ in the case where the Eu f electrons were set in the core. We use a color map to indicate the p-orbital character of the corresponding states, which serves as a visual cue for spotting band inversions. In the Supplementaly Material [43], we compare Fig. 1(c) with the band structure in the case where the putative A-type AFM configuration is assumed, to show that Eu magnetism only perturbs the states close to the Fermi level and therefore does not change the $\mathbb{Z}_2$ index. In Fig. 1(c), there is an evident band inversion, at the Y time-reversal invariant momentum point; however, the nonsymmorphic symmetries force the same four-dimensional representation, $Y_3 + Y_4$, at all states at Y so that $Eu_5In_2Sb_6$ is a trivial insulator. We also verify this using the Check Topological Mat. tool [41,42] on the Bilbao crystallographic server [49–51].

The inset of Fig. 1(c) reproduces the band structure from Rosa *et al.* [20]. In this case, due to a single transcription error [52], the In atom was misplaced along the b axis resulting in heavily distorted tetrahedra with two shorter (In-Sb_1) and two longer (In-Sb_2, In-Sb_3) bonds. An interpolation between the two structures in the absence of SOC (Supplemental Material [43]) shows that as the tetrahedra become more heavily distorted, the character of the lowest conduction bands changes from Eu to In, signaling movement away from the CET limit. In this way, the overlap between conduction and valence bands increases. In the presence of SOC the increased overlap causes a band inversion at Γ making the $\mathbb{Z}_2$ index nontrivial.

Even if these results are negative with respect to $Eu_5In_2Sb_6$ being a magnetic TI, they nevertheless point to the highly tunable band structure of the compound. Indeed, the same kind of distortion of the tetrahedra would occur if we decreased the interlayer distance and/or increased the in-plane bond lengths. Physically, this could be achieved either by applying compressive uniaxial strain along the c axis, or by expanding the a and b lattice constants through epitaxial strain.

To understand why such geometric distortion can cause band inversions, note that in the CET limit, the charge migrates from the Eu atoms to the In_2Sb_6 polyanions. Since the compound has a layered structure with all Eu atoms on the integer layers, most of the accumulated charge will be in the half-integer layers and the system behaves like a dimerized chain along the c axis. We should be careful with this analogy, however, since integer layers also include a Sb_1 atom, so this only applies approximately. Compressing the dimerized chain should move us away from the CET limit by increasing the overlap between conduction and valence bands.

Using DFT, we can simulate the effect of uniaxial strain along the c axis by multiplying the lattice constant c_0 by a coefficient λ^c_{uni} so that the strained lattice constant c is given by $c = \lambda^c_{\text{uni}} c_0$. We then relax the structure but keep c fixed (see Sec. II). Similarly, for epitaxial strain, we keep the in-plane lattice constants $a = \lambda^{ab}_{\text{epi}} a_0$, $b = \lambda^{ab}_{\text{epi}} b_0$ fixed and

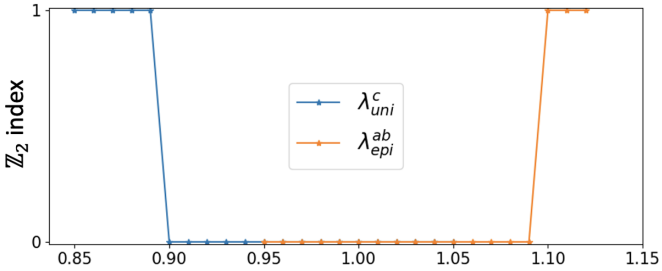

FIG. 2. The $\mathbb{Z}_2$ index of $Eu_5In_2Sb_6$ as a function of epitaxial and uniaxial strain. The $\mathbb{Z}_2$ index becomes nontrivial by either applying compressive uniaxial strain along c or expansive epitaxial strain in the ab plane. Strains of this magnitude are impractical but nevertheless provide insight into the mechanisms that drive Zintl compounds into topological phases.

relax the structure. Figure 2 shows that a 10% compressive uniaxial strain or a 10% expansive epitaxial strain converts the $\mathbb{Z}_2$ index from trivial to nontrivial. Of course, such extreme strains are impractical for any real applications, but these calculations provide insight into mechanisms that can drive Zintl compounds into topological phases. In the Supplemental Material [43], we plot the evolution of the band structure as a function of the strain coefficients, which shows that the effect of displacing the In atom along the b axis is very similar to applying epitaxial and uniaxial strain.

IV. TUNING BAND STRUCTURE PROPERTIES

A. Via chemical substitution

The sensitivity of the band structure to the position of the In atom motivates us to consider its isoelectronic substitution with Ga or Tl. In this way, we can apply chemical pressure while preserving the other properties. After relaxing the substituted structures (both the internal coordinates and lattice constants), we find that the system remains in SG 55 and the phonon frequencies all remain positive, indicating that the structures are dynamically stable (Supplemental Material [43]). In the absence of SOC [Figures 3(a) and 3(b)], the overlap between valence and conduction bands is increased compared to $Eu_5In_2Sb_6$, indicating that $Eu_5Ga_2Sb_6$ and $Eu_5Tl_2Sb_6$ are further away from the CET limit. Just like the case of the displaced In atoms, the lowest conduction states have mostly In-Sb_1 character and the highest valence states have mostly Sb_2-Sb_3 character. We note, however, that in the Ga and Tl substituted compounds the tetrahedra environment is not distorted. When SOC is included a band inversion at Γ occurs, exchanging positive and negative parity eigenvalues [Figs. 3(e) and 3(f)], resulting in a nontrivial $\mathbb{Z}_2$ index. Here considering the putative A-type AFM configuration, Figs. 3(i) and 3(j), does not change the topology and has a small effect on the bulk bands, moving the compounds further away from the CET limit.

Another way to alter the tetrahedra while preserving the chemical properties, is to substitute the Sb in $Eu_5In_2Sb_6$ with

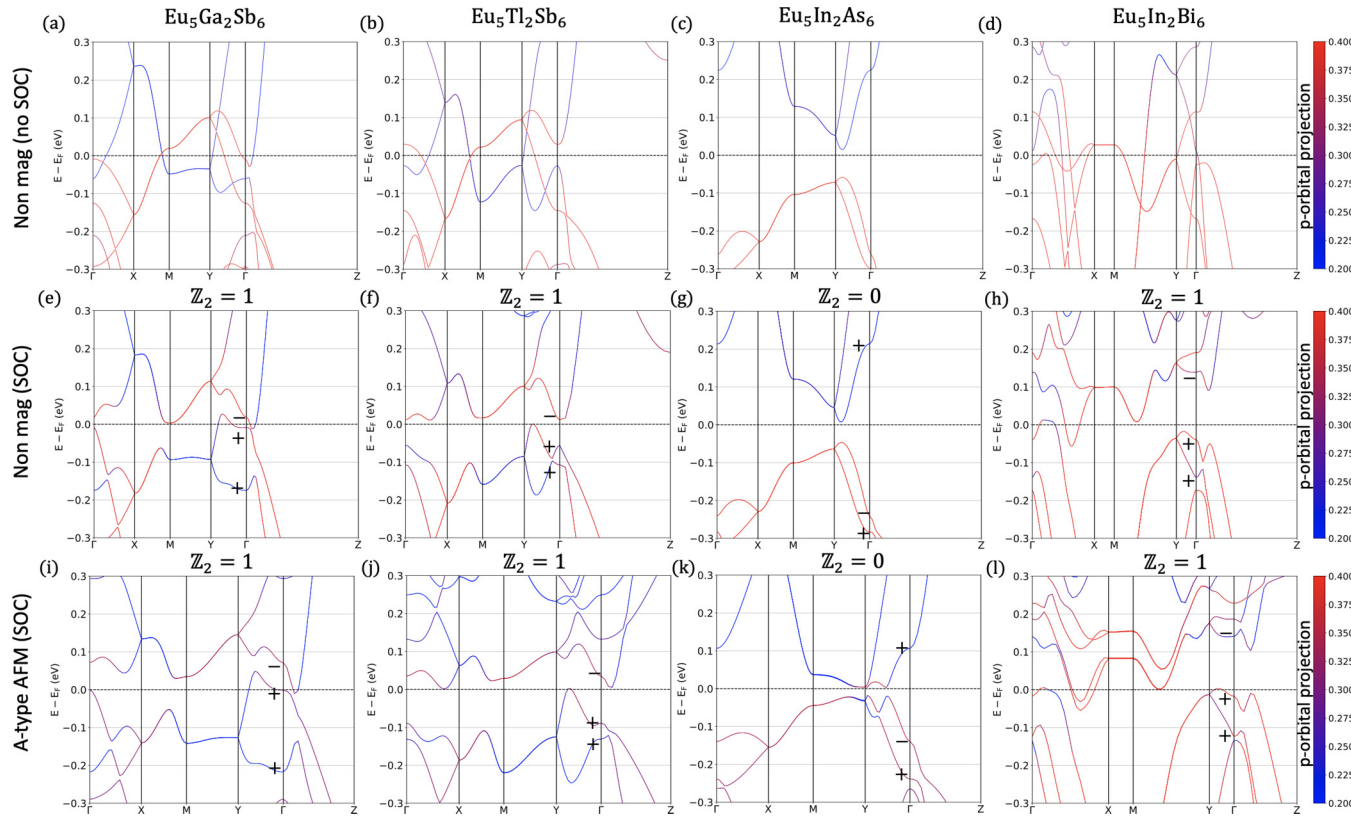

FIG. 3. Band structures (a)–(d) without magnetism and without SOC, (e)–(h) without magnetism and with SOC, and (i)–(l) with an A-type AFM configuration and SOC for the four compounds obtained by isoelectronic substitution of $Eu_5In_2Sb_6$. $Eu_5Ga_2Sb_6$, $Eu_5Tl_2Sb_6$, and $Eu_5In_2Bi_6$ are topologically nontrivial while $Eu_5In_2As_6$ is trivial.

TABLE I. Key properties of the 526 Eu-based Zintls.

Compound	a (Å)	b (Å)	c (Å)	$\mathbb{Z}_2$	Exists?	DG (meV)	IG (meV)
$Eu_5In_2Sb_6$	12.51	14.58	4.62	0	✓	45	23
$Eu_5Ga_2Sb_6$	12.47	14.32	4.54	1	X	16	−39
$Eu_5Tl_2Sb_6$	12.48	14.67	4.70	1	X	70	8
$Eu_5In_2As_6$	11.87	13.78	4.35	0	✓	54	54
$Eu_5In_2Bi_6$	7.77	24.08	4.70	1	✓	77	−69

either As or Bi. Since Sb atoms are three times more abundant than the In atoms and play a central role in determining the polyanion structure, such a substitution has a much more severe effect than substitution by Ga or Tl. Fortunately, both $Eu_5In_2As_6$ [53] and $Eu_5In_2Bi_6$ [54] have been recently synthesized, so their crystallographic structures are known. We find that $Eu_5In_2As_6$ is closer to the CET limit [Fig. 3(c)], and therefore is trivial [Fig. 3(g)]. Instead, $Eu_5In_2Bi_6$ is away from the CET limit [Fig. 3(d)], and has a nontrivial $\mathbb{Z}_2$ index [Fig. 3(h)]. We also verify that the A-type AFM configuration does not have a significant effect on the bulk bands and no effect on the topology [Figs. 3(k) and 3(l).

Table I contains a summary of some of the key features of the 526 compounds discussed. All compounds are in the same space group as the $Eu_5In_2Sb_6$ parent compound. However, $Eu_5In_2Bi_6$ follows a different structure type with modified a and b lattice constants, and the Bi-Bi bond connecting two tetrahedra is now along the a axis instead of the b axis as in the other compounds. With respect to the direct energy gap, the compounds with heavier elements such as Tl or Bi have the largest gap, in part due to the enhanced effect of SOC. In contrast, the indirect or global gap of all nontrivial candidates is negative, with the exception of $Eu_5Tl_2Sb_6$ which has a small indirect gap. Unfortunately, the toxic nature of Tl tends to preclude practical applications. It is therefore desirable to modify the band structures so as to increase the indirect band gap and remove the electron and hole pockets (Fig. 3).

In Sec. V we will discuss the experimental progress towards realizing the magnetic topological insulator in $Eu_5Ga_2Sb_6$.

B. Via strain engineering

We have seen that we can use uniaxial and epitaxial strain to change the topological index by moving away from the CET limit. An important factor in this kind of engineering was the insensitivity of these systems to band inversions other than at the Γ and Z points due to the nonsymmorphic nature of the space group. In this section, we show that moving away from the CET limit can also increase the direct and indirect band gaps. This is much less obvious than changing the topological index, as the gaps are determined by the global band structure properties, i.e., in the whole Brillouin zone. We use $Eu_5In_2Bi_6$ as a case study since the presence of Bi gives rise to larger SOC induced gaps.

Figures 4(a) and 4(b) show that uniaxial strain with $\lambda^a_{\text{uni}} > 1.00$ or $\lambda^c_{\text{uni}} < 1.00$ enhances the direct and indirect gaps. These kinds of uniaxial strain move the compound away from the CET limit by increasing the band overlap (in the absence of SOC). Since we are in the topological phase, a band inversion is required in order to enter the trivial phase. Thus, by moving towards the CET limit we should expect a reduction of the energy gap, while moving away from the CET limit we should expect an enhancement of the energy gap.

In Fig. 4(c) we compare the band structures with $\lambda^c_{\text{uni}} = 1.00$ and $\lambda^c_{\text{uni}} = 0.95$ to illustrate that uniaxial strain can be used to remove electron and hole pockets. The same monotonic behavior occurs with epitaxial strain as we discuss in the Supplemental Material [43]. Finally, because the mechanism is purely electronic and, as we have argued, magnetism occurs on a smaller energy scale, we expect the same monotonic behavior irrespective of the magnetic configuration.

V. EXPERIMENTAL PROGRESS

Motivated by the strong theoretical predictions of magnetic topological insulating states in $Eu_5Ga_2Sb_6$, we attempted its preparation following known synthetic recipes for $Eu_5In_2Sb_6$ [20,28,55]. In agreement with prior reports [55], we were unable to find synthetic conditions in which to stabilize the Ga phase. Prior work on topological insulators has shown that solid solutions are a viable avenue to tune across topological phase transitions, e.g., $Bi_{1-x}Sb_x$ [56,57] and $TlBiS_{2-x}Se_x$ [58]. With this in mind, we utilized polycrystalline synthesis to find the solid solubility limit of Ga in $Eu_5In_{2-x}Ga_xSb_6$.

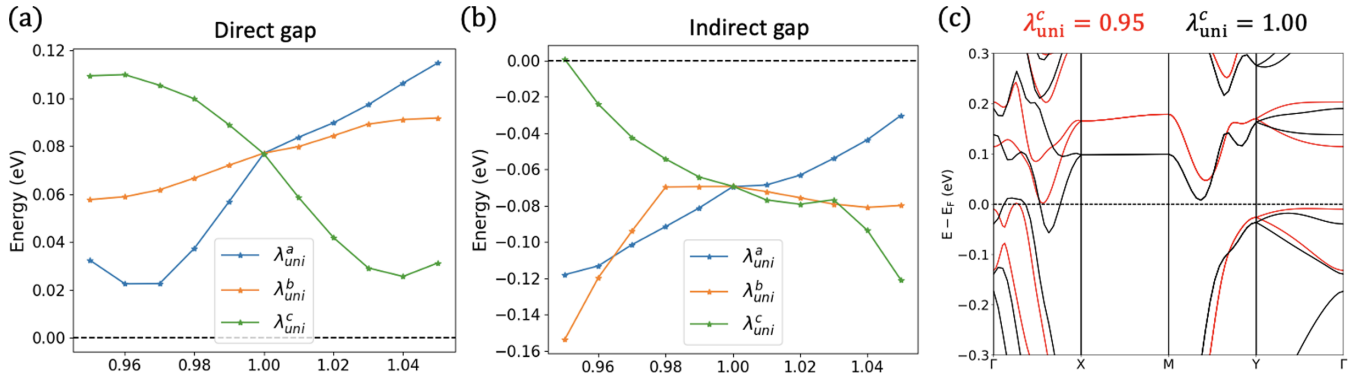

FIG. 4. Effect of uniaxial strain on (a) direct and (b) indirect gaps. (e) Comparison between band structures with $\lambda^c_{\text{uni}} = 1.00$ and $\lambda^c_{\text{uni}} = 0.95$.

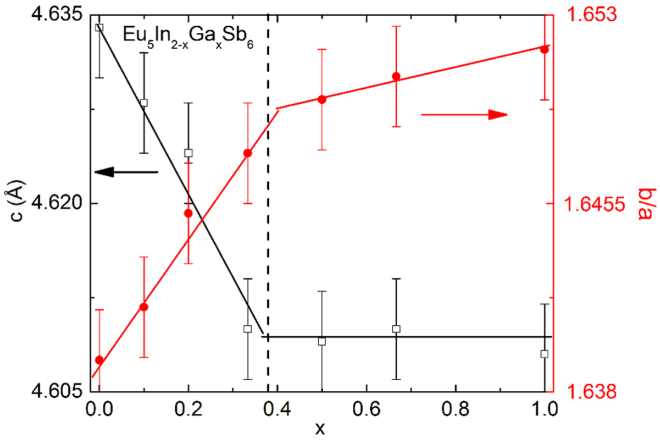

FIG. 5. The c axis and b/a ratio of polycrystalline $Eu_5In_{2-x}Ga_xSb_6$ show a systematic evolution with Ga substitution up to $x \approx 0.4$, the apparent solid solubility limit. Contraction of the c lattice constant with increased Ga concentration indicates movement away from the CET limit, in agreement with the DFT prediction.

Figure 5 summarizes our findings. As the structure of $Eu_5In_2Sb_6$ is orthorhombic, with chains of $(In/Ga)Sb_4$ tetrahedra aligned along the c axis, we find an expected contraction along the c axis, and a smaller change in the ab plane where the tetrahedra slightly contract, but retain optimum bonding environments for Eu. Specifically the c lattice parameter decreases from 4.634 Å to a minimum of 4.608 Å. The a lattice parameter decreases slightly from 12.530 Å to 12.520 Å over the same range, while b is unchanged within error (14.584 Å at $x = 0$). This contraction of the c axis should push the material further away from the CET limit and towards a topological state. Further evidence for successful substitution comes from the monotonic increase in the b/a ratio over the same composition range, implying a change in the relative shape in the ab plane. This demonstrates that partial replacement of In with Ga is possible, and motivates further work to both extend the phase stability line, and determine whether there is experimentally a change in topology in the chemically accessible range.

In addition, future work includes the synthesis of $Eu_5In_2Bi_6$ single crystals utilizing the flux technique. Prior works suggest the existence of $Eu_5In_2Bi_6$ in polycrystalline form, but as a minority phase, and phase purity could not be achieved [54]. By utilizing the flux technique we hope to segregate the thermodynamically unstable, $Eu_5In_2Bi_6$ phase in the single-crystal form. The single crystals would also allow us to understand the nature of transport and magnetism in $Eu_5In_2Bi_6$ and allow us to explore new avenues to the discovery of magnetic topological states of matter.

VI. SUMMARY AND CONCLUSIONS

The Zintl concept is an example of a chemical concept that provides a bridge between the structural and electronic properties for a particular class of compounds. This is especially interesting for the engineering of topological insulators, which require inverted insulating gaps. In addition, the large number of Zintl compounds that have been synthesized means that there is a big enough search space to allow optimization of desired properties such as bulk and surface gaps. DFT is an indispensable tool in this search, since it allows accurate prediction of material properties.

In this work, we gain a deeper understanding into how structural and electronic properties interact in the 526 family of Eu-based Zintl compounds. We use the Zintl concept to relate the layered structure to an ionic chain along c. By realizing that we need to move away from the CET limit, we find ways to change the topology and remove electron and hole pockets. These insights will be applicable in various other systems of Zintl compounds. For example, it was recently predicted that the Eu-based Zintl $EuCd_2Sb_2$ [59] becomes a 2D AFM TI under tensile strain. This is explained by the same mechanism we described here as all divalent Eu atoms are located in a single layer as for the 526 Zintls.

Finally we note that, due to the highly tunable energy gap in Zintls, whether the proposed candidates will have gapped bulk and surface gaps will depend sensitively on the crystal structure and the magnetic configuration. Therefore, the aim of this work is to show and explain trends and provide motivation for further investigation and not to make quantitative predictions.

Polycrystalline $Eu_5In_{2-x}Ga_xSb_6$ were prepared in a manner similar to that previously reported for $Eu_5In_2Sb_6$, with equimolal replacement of In with Ga [28,55]. Powder x-ray diffraction patterns were collected over an angular range of 5°–90° 2θ on a Bruker D8 focus equipped with a LynxEye detector, 1 mm incident slit, Soller slits, and an air antiscatter shield, and indexed using Lebail refinements as implemented in Bruker TOPAS.

ACKNOWLEDGMENTS

We acknowledge constructive discussions with N. Peter Armitage, C. Broholm, V. Morano, P. Rosa, Y. Xu, Z. Wang, and A. Bernevig. N.V. thanks S. Singh for teaching him how to perform phonon calculations and providing the VASP code to perform epitaxial and uniaxial strain calculations. This work was supported as part of the Institute for Quantum Matter, an Energy Frontier Research Center funded by the U.S. Department of Energy, Office of Science, Basic Energy Sciences under Award No. DE-SC0019331.

[1] M. Z. Hasan and C. L. Kane, *Colloquium*: Topological insulators, Rev. Mod. Phys., **82**, 3045 (2010).

[2] X.-L. Qi and S.-C. Zhang, Topological insulators and superconductors, Rev. Mod. Phys. **83**, 1057 (2011).

[3] X. L. Qi, T. L. Hughes, and S. C. Zhang, Topological field theory of time-reversal invariant insulators, Phys. Rev. B **78**, 195424 (2008).

[4] A. M. Essin, J. E. Moore, and D. Vanderbilt, Magnetoelectric Polarizability and Axion Electrodynamics in Crystalline Insulators, Phys. Rev. Lett. **102**, 146805 (2009); **103**, 259902 (2009).

[5] N. Varnava, I. Souza, and D. Vanderbilt, Axion coupling in the hybrid Wannier representation, Phys. Rev. B **101**, 155130 (2020).

[6] K. Yasuda, M. Mogi, R. Yoshimi, A. Tsukazaki, K. S. Takahashi, M. Kawasaki, F. Kagawa, and Y. Tokura, Quantized chiral edge conduction on domain walls of a magnetic topological insulator, Science **358**, 1311 (2017).

[7] E. Khalaf, Higher-order topological insulators and superconductors protected by inversion symmetry, Phys. Rev. B **97**, 205136 (2018).

[8] N. Varnava and D. Vanderbilt, Surfaces of axion insulators, Phys. Rev. B **98**, 245117 (2018).

[9] N. Varnava, J. H. Wilson, J. H. Pixley, and D. Vanderbilt, Controllable quantum point junction on the surface of an antiferromagnetic topological insulator, Nat. Commun. **12**, 3998 (2021).

[10] Y. Tokura, K. Yasuda, and A. Tsukazaki, Magnetic topological insulators, Nat. Rev. Phys. **1**, 126 (2019).

[11] P. Wang, J. Ge, J. Li, Y. Liu, Y. Xu, and J. Wang, Intrinsic magnetic topological insulators, The Innovation **2**, 100098 (2021).

[12] B. A. Bernevig, C. Felser, and H. Beidenkopf, Progress and prospects in magnetic topological materials, Nature (London) **603**, 41 (2022).

[13] M. M. Otrokov, I. I. Klimovskikh, H. Bentmann, D. Estyunin, A. Zeugner, Z. S. Aliev, S. Gaß, A. U. B. Wolter, A. V. Koroleva, A. M. Shikin, M. Blanco-Rey, M. Hoffmann, I. P. Rusinov, A. Yu. Vyazovskaya, S. V. Eremeev, Yu. M. Koroteev, V. M. Kuznetsov, F. Freyse, J. Sánchez-Barriga, I. R. Amiraslanov *et al.*, Prediction and observation of an antiferromagnetic topological insulator, Nature (London) **576**, 416 (2019).

[14] J. Li, Y. Li, S. Du, Z. Wang, B.-L. Gu, S.-C. Zhang, K. He, W. Duan, and Y. Xu, Intrinsic magnetic topological insulators in van der Waals layered $MnBi_2Te_4$-family materials, Sci. Adv. **5** (2019).

[15] Y. Xu, Z. Song, Z. Wang, H. Weng, and X. Dai, Higher-Order Topology of the Axion Insulator $EuIn_2As_2$, Phys. Rev. Lett. **122**, 256402 (2019).

[16] H. Li, S.-Y. Gao, S.-F. Duan, Y.-F. Xu, K.-J. Zhu, S.-J. Tian, J.-C. Gao, W.-H. Fan, Z.-C. Rao, J.-R. Huang, J.-J. Li, D.-Y. Yan, Z.-T. Liu, W.-L. Liu, Y.-B. Huang, Y.-L. Li, Y. Liu, G.-B. Zhang, P. Zhang, T. Kondo *et al.*, Dirac Surface States in Intrinsic Magnetic Topological Insulators $EuSn_2As_2$ and $MnBi_{2n}Te_{3n+1}$, Phys. Rev. X **9**, 041039 (2019).

[17] I. I. Klimovskikh, M. M. Otrokov, D. Estyunin, S. V. Eremeev, S. O. Filnov, A. Koroleva, E. Shevchenko, V. Voroshnin, A. G. Rybkin, I. P. Rusinov, M. Blanco-Rey, M. Hoffmann, Z. S. Aliev, M. B. Babanly, I. R. Amiraslanov, N. A. Abdullayev, V. N. Zverev, A. Kimura, O. E. Tereshchenko, K. A. Kokh *et al.*, Tunable 3Dd/2D magnetism in the $(MnBi_2Te_4)(Bi2Te_3)_m$ topological insulators family, npj Quantum Mater. **5**, 54 (2020).

[18] J. Ma, H. Wang, S. Nie, C. Yi, Y. Xu, H. Li, J. Jandke, W. Wulfhekel, Y. Huang, D. West, P. Richard, A. Chikina, V. N. Strocov, J. Mesot, H. Weng, S. Zhang, Y. Shi, T. Qian, M. Shi, and H. Ding, Emergence of nontrivial low-energy Dirac fermions in antiferromagnetic $EuCd_2As_2$, Adv. Mater. **32**, 1907565 (2020).

[19] Y. Xu, L. Elcoro, Z.-D. Song, B. J. Wieder, M. G. Vergniory, N. Regnault, Y. Chen, C. Felser, and B. A. Bernevig, High-throughput calculations of magnetic topological materials, Nature (London) **586**, 702 (2020).

[20] P. Rosa, Y. Xu, M. Rahn, J. Souza, S. Kushwaha, L. Veiga, A. Bombardi, S. Thomas, M. Janoschek, E. Bauer, M. Chan, Z. Wang, J. Thompson, N. Harrison, P. Pagliuso, A. Bernevig, and F. Ronning, Colossal magnetoresistance in a nonsymmorphic antiferromagnetic insulator, npj Quantum Mater. **5**, 52 (2020).

[21] G. M. Pierantozzi, A. De Vita, C. Bigi, X. Gui, H.-J. Tien, D. Mondal, F. Mazzola, J. Fujii, I. Vobornik, G. Vinai, A. Sala, C. Africh, T.-L. Lee, G. Rossi, T.-R. Chang, W. Xie, R. J. Cava, and G. Panaccione, Evidence of magnetism-induced topological protection in the axion insulator candidate $EuSn_2P_2$, Proc. Natl. Acad. Sci. USA **119**, e2116575119 (2022).

[22] Y. Deng, Y. Yu, M. Z. Shi, Z. Guo, Z. Xu, J. Wang, X. H. Chen, and Y. Zhang, Quantum anomalous Hall effect in intrinsic magnetic topological insulator $MnBi_2Te_4$, Science **367**, 895 (2020).

[23] C. Liu, Y. Wang, H. Li, Y. Wu, Y. Li, J. Li, K. He, Y. Xu, J. Zhang, and Y. Wang, Robust axion insulator and Chern insulator phases in a two-dimensional antiferromagnetic topological insulator, Nat. Mater. **19**, 522 (2020).

[24] S. M. Kauzlarich, A. Zevalkink, E. Toberer, and G. J. Snyder, Chapter 1 Zintl phases: Recent developments in thermoelectrics and future outlook, *Thermoelectric Materials and Devices* (The Royal Society of Chemistry, London, 2017), pp. 1–26

[25] L. Deakin, R. Lam, F. Marsiglio, and A. Mar, Superconductivity in $Ba_2Sn_3Sb_6$ and $SrSn_3Sb_4$, J. Alloys Compd. **338**, 69 (2002), special Issue to Honor Professor H. Fritz Franzen.

[26] J. Y. Chan, S. M. Kauzlarich, P. Klavins, R. N. Shelton, and D. J. Webb, Colossal magnetoresistance in the transition-metal Zintl compound $Eu_{14}MnSb_{11}$, Chem. Mater. **9**, 3132 (1997).

[27] K.-F. Liu and S.-Q. Xia, Recent progresses on thermoelectric Zintl phases: Structures, materials and optimization, J. Solid State Chem. **270**, 252 (2019).

[28] S.-M. Park, E. S. Choi, W. Kang, and S.-J. Kim, $Eu_5In_2Sb_6$, $Eu_5In_{2-x}Zn_xSb_6$: Rare earth zintl phases with narrow band gaps, J. Mater. Chem. **12**, 1839 (2002).

[29] P. Hohenberg and W. Kohn, Inhomogeneous Electron Gas, Phys. Rev. **136**, B864 (1964).

[30] W. Kohn and L. J. Sham, Self-Consistent Equations Including Exchange and Correlation Effects, Phys. Rev. **140**, A1133 (1965).

[31] G. Kresse and J. Furthmüller, Efficient iterative schemes for *ab initio* total-energy calculations using a plane-wave basis set, Phys. Rev. B **54**, 11169 (1996).

[32] G. Kresse and D. Joubert, From ultrasoft pseudopotentials to the projector augmented-wave method, Phys. Rev. B **59**, 1758 (1999).

[33] J. P. Perdew, K. Burke, and M. Ernzerhof, Generalized Gradient Approximation Made Simple, Phys. Rev. Lett. **77**, 3865 (1996).

[34] A. Togo and I. Tanaka, First principles phonon calculations in materials science, Scr. Mater. **108**, 1 (2015).

[35] J. Gao, Q. Wu, C. Persson, and Z. Wang, Irvsp: To obtain irreducible representations of electronic states in the VASP, Comput. Phys. Commun. **261**, 107760 (2021).

[36] U. Herath, P. Tavadze, X. He, E. Bousquet, S. Singh, F. Muñoz, and A. H. Romero, PyProcar: A Python library for electronic structure pre/post-processing, Comput. Phys. Commun. **251**, 107080 (2020).

[37] L. Fu and C. L. Kane, Topological insulators with inversion symmetry, Phys. Rev. B **76**, 045302 (2007).

[38] J. Kruthoff, J. de Boer, J. van Wezel, C. L. Kane, and R.-J. Slager, Topological Classification of Crystalline Insulators through Band Structure Combinatorics, Phys. Rev. X **7**, 041069 (2017).

[39] B. Bradlyn, L. Elcoro, J. Cano, M. G. Vergniory, Z. Wang, C. Felser, M. I. Aroyo, and B. A. Bernevig, Topological quantum chemistry, Nature (London) **547**, 298 (2017).

[40] H. C. Po, A. Vishwanath, and H. Watanabe, Symmetry-based indicators of band topology in the 230 space groups, Nat. Comunn. **8**, 50 (2017).

[41] M. G. Vergniory, L. Elcoro, C. Felser, N. Regnault, B. A. Bernevig, and Z. Wang, A complete catalogue of high-quality topological materials, Nature (London) **566**, 480 (2019).

[42] M. G. Vergniory, B. J. Wieder, L. Elcoro, S. S. P. Parkin, C. Felser, B. A. Bernevig, and N. Regnault, All topological bands of all stoichiometric materials, Science **376**, 6595 (2022).

[43] See Supplemental Material at http://link.aps.org/supplemental/10.1103/PhysRevB.105.235128 for additional calculations.

[44] M. Yu, S. Yang, C. Wu, and N. Marom, Machine learning the Hubbard U parameter in DFT+U using Bayesian optimization, npj Comput. Mater. **6**, 180 (2020).

[45] Y. Chen, H.-S. Kim, and H.-Y. Kee, Topological crystalline semimetals in nonsymmorphic lattices, Phys. Rev. B **93**, 155140 (2016).

[46] B. J. Wieder, B. Bradlyn, Z. Wang, J. Cano, Y. Kim, H.-S. D. Kim, A. M. Rappe, C. L. Kane, and B. A. Bernevig, Wallpaper fermions and the nonsymmorphic dirac insulator, Science **361**, 246 (2018).

[47] M. G. Vergniory, L. Elcoro, Z. Wang, J. Cano, C. Felser, M. I. Aroyo, B. A. Bernevig, and B. Bradlyn, Graph theory data for topological quantum chemistry, Phys. Rev. E **96**, 023310 (2017).

[48] L. Elcoro, B. Bradlyn, Z. Wang, M. G. Vergniory, J. Cano, C. Felser, B. A. Bernevig, D. Orobengoa, G. de la Flor, and M. I. Aroyo, Double crystallographic groups and their representations on the Bilbao Crystallographic Server, J. Appl. Crystallogr. **50**, 1457 (2017).

[49] M. I. Aroyo, A. Kirov, C. Capillas, J. M. Perez-Mato, and H. Wondratschek, Bilbao Crystallographic Server. II. Representations of crystallographic point groups and space groups, Acta Crystallogr., Sect. A: Found. Adv. **62**, 115 (2006).

[50] M. I. Aroyo, J. M. Perez-Mato, C. Capillas, E. Kroumova, S. Ivantchev, G. Madariaga, A. Kirov, and H. Wondratschek, Bilbao crystallographic server: I. Databases and crystallographic computing programs, Z. Kristallogr. - Cryst. Mater. **221**, 15 (2006).

[51] M. I. Aroyo, J. Perez-Mato, D. Orobengoa, E. Tasci, G. De la Flor Martin, and A. Kirov, Crystallography online: Bilbao crystallographic server, Bulg. Chem. Commun. **43**, 183 (2011).

[52] $y_{\mathrm{In}} = 0.2419$ was used in their calculation while $y_{\mathrm{In}} = 0.2149$ is reported in Park *et al.* [28].

[53] A. B. Childs, S. Baranets, and S. Bobev, Five new ternary indium-arsenides discovered. Synthesis and structural characterization of the Zintl phases $Sr_3In_2As_4$, $Ba_3In_2As_4$, $Eu_3In_2As_4$, $Sr_5In_2As_6$ and $Eu_5In_2As_6$, J. Solid State Chem. **278**, 120889 (2019).

[54] M. Radzieowski, F. Stegemann, S. Klenner, Y. Zhang, B. P. T. Fokwa, and O. Janka, On the divalent character of the Eu atoms in the ternary Zintl phases $Eu_5In_2Pn_6$ and Eu_3MAs_3 (Pn = As-Bi; M = Al,Ga), Mater. Chem. Front. **4**, 1231 (2020).

[55] U. Subbarao, S. Sarkar, B. Joseph, and S. C. Peter, Magnetic and X-ray absorption studies on the $RE_5X_2Sb_6$ (RE=Eu, Yb; X=Al, Ga, In) compounds, J. Alloys Compd. **658**, 395 (2016).

[56] J. C. Y. Teo, L. Fu, and C. L. Kane, Surface states and topological invariants in three-dimensional topological insulators: Application to $Bi_{1-x}Sb_x$, Phys. Rev. B **78**, 045426 (2008).

[57] D. Hsieh, D. Qian, L. Wray, Y. Xia, Y. S. Hor, R. J. Cava, and M. Z. Hasan, A topological dirac insulator in a quantum spin Hall phase, Nature (London) **452**, 970 (2008).

[58] T. Sato, K. Segawa, K. Kosaka, S. Souma, K. Nakayama, K. Eto, T. Minami, Y. Ando, and T. Takahashi, Unexpected mass acquisition of Dirac fermions at the quantum phase transition of a topological insulator, Nat. Phys. **7**, 840 (2011).

[59] R. Li, H. Wang, N. Mao, H. Ma, B. Huang, Y. Dai, and C. Niu, Engineering antiferromagnetic topological insulator by strain in two-dimensional rare-earth pnictide $EuCd_2Sb_2$, Appl. Phys. Lett. **119**, 173105 (2021).